Hydrogen Recombination Lines in the Compact HII Region K3-50a

Phil Puxley
Gemini 8m Telescopes Project, 950 N. Cherry Ave., Tucson AZ 85719

Gemini Preprint # 25

Hydrogen Recombination Lines in the Compact HII Region K3-50a

Phil Puxley

Gemini 8m Telescopes Project, 950 N. Cherry Ave., Tucson, AZ 85741. USA.

Abstract. New observations of hydrogen recombination lines in the compact HII region K3-50a are presented. They cover a broad wavelength range from the near-IR (Brα and others, observed with ISO), through sub-mm and mm transitions (H26α - H30α from JCMT and H40α - H68α from Nobeyama) to radio wavelengths. The line fluxes are compared with a simple model.

Keywords: HII regions, recombination lines, emission mechanisms

1. Introduction and observations

As part of a study of hydrogen recombination line emission processes in dusty HII regions, new observations have been made of the compact source K3-50a. The observed transitions cover a broad wavelength range from the near-IR (observed with ISO), through the sub-mm and mm (JCMT and Nobeyama 45m) to radio wavelengths. The complete list of newly detected transitions, together with existing radio data, is given in Table 1. Other sources included in this multi-wavelength study are G29.96, G45.12 and, for comparison purposes, the planetary nebula NGC7027.

Table 1. Hydrogen recombination line data for K3-50a.

line	telescope	frequency (GHz)	peak flux density (Jy)	reference
Brα	ISO	73981	340 ± 85	new
Pfα	ISO	40187	216 ± 54	new
Huα	ISO	24232	tbd	new
H7α	ISO	15727	tbd	new
H8α	ISO	10783	tbd	new
H26α	JCMT	353.6	8.9 ± 1.1	new
H27α	JCMT	316.4	10.8 ± 1.3	new
H29α	JCMT	256.3	7.5 ± 0.6	new
H30α	JCMT	231.9	7.2 ± 0.6	new
H40α	NRO	99.0	3.7 ± 0.4	new
H42α	NRO	85.7	3.0 ± 0.4	new
H53α	NRO	42.9	2.1 ± 0.2	new
H57α	NRO	34.6	1.7 ± 0.2	new
H66α	NRO	22.4	1.1 ± 0.1	new
H68α	NRO	20.5	1.0 ± 0.1	new
H76α	VLA	14.7	0.48 ± 0.10	De Pree et al. (1994)
H109α	WSRT	5.0	0.072 ± 0.008	Van Gorkom et al. (1981)
H110α	WSRT	4.9	0.058 ± 0.008	Roelfsema et al. (1988)

Several illustrative spectra are shown in Fig. 1. The sub-mm and mm antenna temperatures were converted to flux densities assuming a source FWHM of 2.2 arcsec (De Pree et al. 1994) leading to beam correction factors of 1-3%. The uncertainties quoted in the table are the quadratic sum of uncertainties in the peak flux density from a single Gaussian fit, beam size and telescope aperture efficiency. The ISO data have only been partially analysed and an absolute calibration uncertainty of 25% has been assigned.

2. Line emission processes

Shown in Fig. 2 are the recombination line observations and an ad hoc nebula model. The model incorporates spontaneous and stimulated emission for the Case B approximation and uses departure coefficients from Salem and Brocklehurst (1979) and Walmsley (1990) to describe the departure of the level populations from LTE. The general expression for the peak total line flux density in such a model (e.g. Bell & Seaquist 1978; Puxley et al. 1991), in the absence of stimulated emission by a background source, is

$$S_L^{tot} = \Omega B(\nu_L, T_e)\left[\left(\frac{\tau_c + b_n \tau_L^*}{\tau_c + \gamma \tau_L^* b_n}\right)\left(1 - e^{-(\tau_L + \tau_c)}\right) - \left(1 - e^{-\tau_c}\right)\right]$$

where Ω is the solid angle subtended by the source, B is the Planck function, τ_c and τ_L are the continuum and line optical depths, τ_L^* is the LTE line optical depth, and b_n and γ describe the departure from LTE. In the example illustrated above, of purely spontaneous emission, this expression reduces to

$$S_L^{spont} = \Omega B(\nu_L, T_e) e^{-\tau_c}(1 - e^{-\tau_L})$$

These simplified models are characterised by the source size, as expressed by Ω, and the electron temperature and density, which define the dependence of departure coefficients on principal quantum number. It can be seen that this model is in good overall agreement with the data.

The toy model illustrated in Fig. 2 does not yet include the several effects of dust. Absorption of line photons by dust at the shorter wavelengths is well known. However absorption of UV photons, by dust internal to the nebula, can also reduce the line optical depth of Lyman transitions, causing the level population to revert from Case B (optically thick) to Case A. Thermal emission from the warm internal dust can induce transitions between high bound levels via absorption and stimulated emission. These latter two processes have been studied by Hummer & Storey (1992) and each can cause a deviation of 15-25% from Case B.

Following completion of the ISO SWS data processing, more realistic source models are to be constructed, incorporating the shell morphologies and velocity gradients exhibited by several of the targets, and the multi-wavelength dataset will be analysed to quantify the departures from LTE and the Case B approximation.

Acknowledgements. Thanks are due to collaborators on aspects of this project: Peter Brand (University of Edinburgh), Toby Moore (Liverpool John Moores University), Matt Mountain (Gemini 8m Telescopes) and Naomasa Nakai (Nobeyama Radio Observatory), and to Pat Roche for assistance with some of the

NRO observations. We are grateful to the support staff of the JCMT, NRO45m and ISO data entry (PDEC) and processing (IPAC) centres.

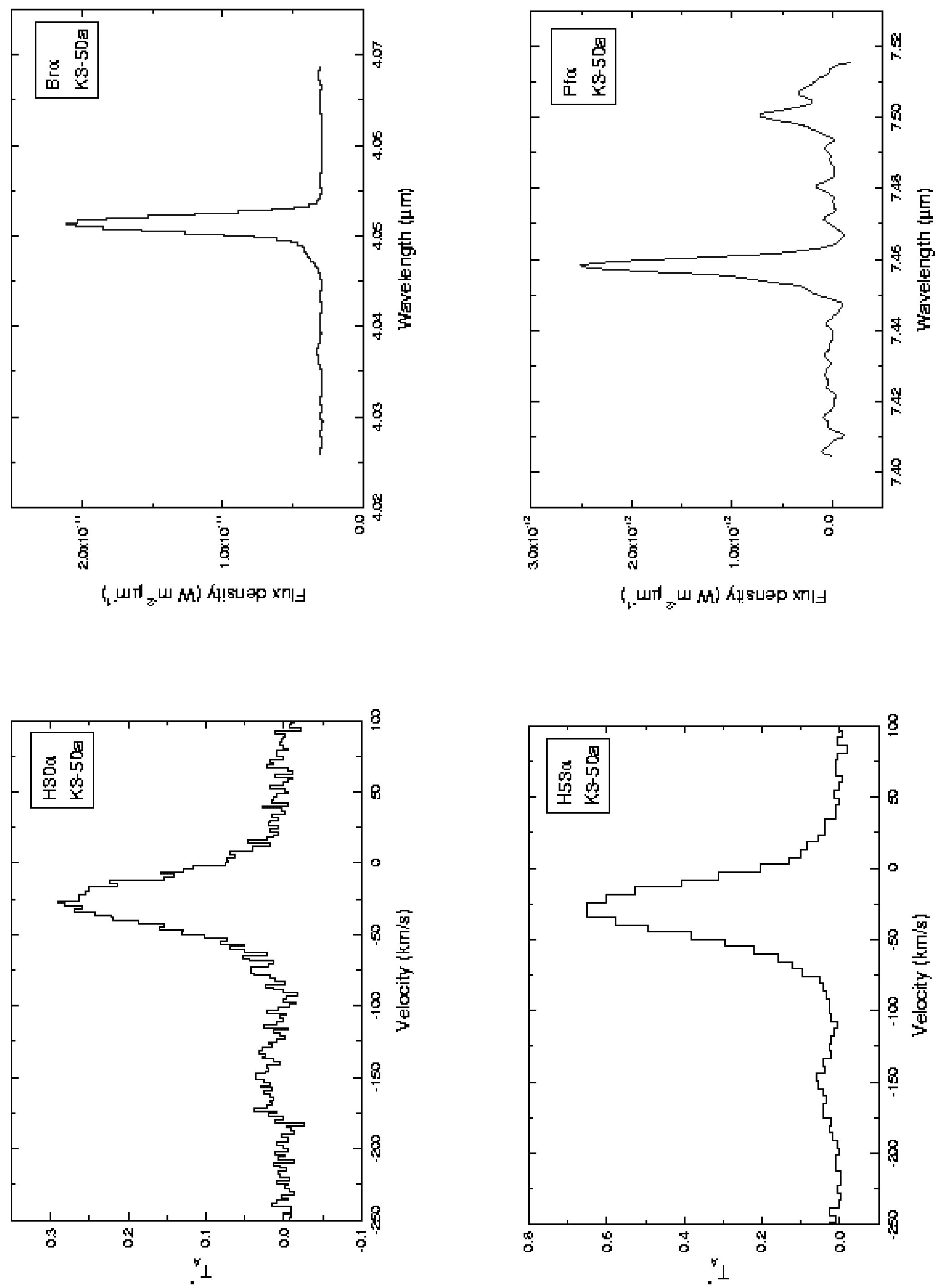

Figure 1. Example spectra of K3-50a: H30α, H53α, Brα and Pfα.

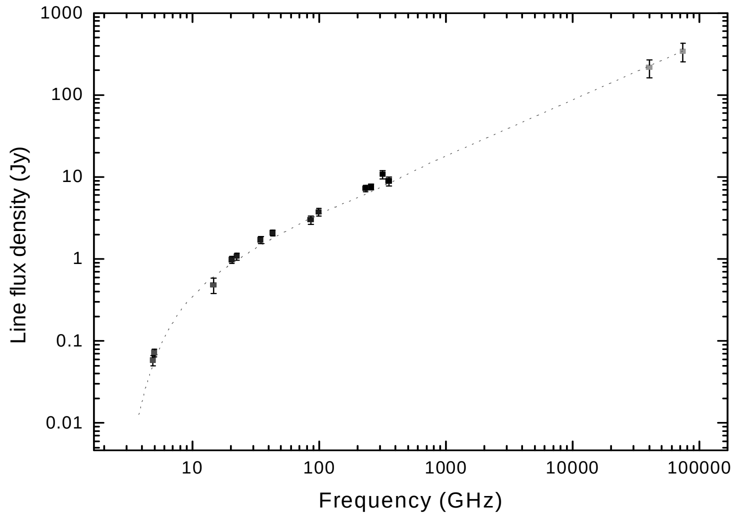

Figure 2. Simple model of the K3-50a line emission and observational data.

References

Bell, M.B., & Seaquist, E.R. 1978, ApJ, 223, 378
De Pree, C.G., Goss, W.M., Palmer, P., & Rubin, R.H. 1994, ApJ, 428, 670
Hummer, D.G., & Storey, P.J. 1992, MNRAS, 254, 277
Puxley, P.J., Brand, P.W.J.L., Moore, T.J.T., Mountain, C.M., & Nakai, N. 1991, MNRAS, 248, 585
Roelfsema, P.R., Goss, W.M., & Geballe, T.R. 1988, A&A, 207, 132
Salem, M., & Brocklehurst, M. 1979, ApJS, 39, 633
Van Gorkom, J.H., Shaver, P.A., Pottasch, S.R., Blair, G.N., Matthews, H.E. 1981, A&A, 94, 259
Walmsley, C.M. 1990. A&AS, 82, 201